1983ApJ...264..432S

THE ASTROPHYSICAL JOURNAL, 264:432–445, 1983 January 15
© 1983. The American Astronomical Society. All rights reserved. Printed in U.S.A.

BUBBLES, JETS, AND CLOUDS IN ACTIVE GALACTIC NUCLEI

MICHAEL D. SMITH
Department of Physics, University of Illinois at Urbana-Champaign; and University of Maryland
LARRY SMARR
Department of Astronomy, University of Illinois at Urbana-Champaign
MICHAEL L. NORMAN
Max-Planck-Institut für Physik und Astrophysik, Garching, München
AND
JAMES R. WILSON
Lawrence Livermore Laboratory
Received 1981 May 14; accepted 1982 July 2

ABSTRACT

The Blandford and Rees 1974 fluid twin-exhaust model for jet formation is thoroughly investigated. We perform detailed analytic calculations of all aspects of the cavity-nozzle structures for the nonrelativistic case: the preshock flow, the central shock, cavity flow, and the nozzle. Our analytic results are in excellent agreement with recent sophisticated numerical calculations. We find that for a given central confining gas cloud, only a finite range of jet powers is possible. The sound speed ratio between cavity and cloud must be less than 30. Central masses of $\sim 10^9\ M_\odot$ within 1 pc are necessary for high-powered (10^{46} ergs s^{-1}) extragalactic jets.

For a fixed confining cloud sound speed C_0, there are three regimes determined by the central engine's luminosity. For low luminosity, a stream of bubbles emerges; for a middle range of luminosities, a jet forms; for too high a luminosity, large clouds are emitted. In the jet regime we find that $L_j \sim C_0^5$.

The critical dependence of jet power on confining cloud sound speed enables a schematic picture for active galactic nuclei to be proposed. Seyfert galaxies and quasars are placed in the bubble regime. Variable compact radio sources reach the cloud regime. Evolutionary paths are suggested and may provide an indirect test for this picture.

Subject headings: galaxies: nuclei — particle acceleration

I. INTRODUCTION

Various attempts have been made to simulate active galactic nuclei and extended radio sources by studying the motions of high energy gas produced from a point source. The conclusions are rather disjoint owing to the numerous possible effects and assumptions that can be considered or ignored in modeling three-dimensional gas flows. For instance, Gull and Northover (1973) concluded that the energy is released through bubbles of hot gas that rise out of the nucleus along the axis of rotation. However, their analysis only considered the large scale instabilities when confining a growing central cavity of hot gas by a denser external medium. Blandford and Rees (1974) proposed that the energy is released continuously through "twin exhausts," although the question of instabilities was left open. Numerical integrations ("$1\frac{1}{2}$" dimensional) by Wiita (1978*b*) appear to tie these two conflicting hypotheses together. He found a critical source luminosity that separates bubble and jet formation. This work took into rough consideration the Rayleigh-Taylor instability of the central cavity and ignored the Kelvin-Helmholtz instability between the jet flow and the nuclear gas cloud. Wiita (1978*a*) refined the Blandford and Rees model by taking a more compact central cloud, while keeping the one-dimensional flow approximation. Rayburn (1977) made some coarse grid two-dimensional hydrodynamic calculations on the early stages of jet formation.

The above investigations assumed that hot gas is continuously injected into a central cavity within a relatively cool, dense central cloud. Explosions in galactic nuclei were considered by Sanders (1976). A simple analysis demonstrated that axisymmetric flow or central blast waves can occur, dependent on the mass released in the explosion. Relativistic blast waves have been considered by Blandford and McKee (1977) and Shapiro (1979), while axisymmetric flow was discussed by Christiansen and Scott (1977). Observations of active galactic nuclei indicate that both steady activity and explosions occur.

© American Astronomical Society • Provided by the NASA Astrophysics Data System

1983ApJ...264..432S

We shall look to the nonrelativistic fluid flow version of the Blandford and Rees twin-exhaust model to produce steady flows. Sophisticated two-dimensional numerical simulations (Norman *et al.* 1981) have revealed a number of flow characteristics that were not previously taken into account. The instabilities and the initial approach to a steady flow (where it exists) can result in fast changes of the central structure. In this manner, the study is atuned to both rapid variability and steady flows.

Our analysis will be presented in the following order. The initial turn-on of the hot gas and the expanding "cavity" of hot gas are discusssed in § II. We determine the escape route of this buoyant gas. In § III the stability of the escape routes—the nozzles—is analyzed. In § IV we investigate the stability of the cavity. These results are fully described in § V. In § VI various applications are considered, and we introduce a schematic picture based on the three gas escape mechanisms—small bubbles, jets, and large clouds. In §§ VII and VIII, the properties of the bubbles and clouds are calculated, and their effect on the schematic picture is elaborated. Section IX contains a summary of our results.

II. STEADY EXPANSION

We begin by setting up the necessary formalism and discuss the approach to the basic flow pattern as shown in Figure 1.

A nuclear gas cloud with pressure $p_m(R, Z)$ decreasing with increasing R and Z, the coordinates of a cylindrical coordinate system, is presumed. The nucleus will also contain a distribution of stars or other dense massive objects that contribute only to the gravitational potential. The nucleus will be more clearly specified in following sections.

A high pressure, p_e, extremely hot (nonrelativistic) gas is "turned on" and is then steadily produced from a "central engine" of small dimension, r_e. This gas will be treated as an adiabatic, inviscid fluid except at shocks. The hot gas drives out the surrounding dense cloud, and an expanding cavity of hot gas results. The initial evacuation, described in detail by Wiita (1978*b*), is very rapid due to the high pressure gradients, and the flow quickly becomes supersonic. Once the external gas is driven out, the radial expansion close to the engine will approach spherical symmetry. Consequently a steady supersonic outflow is attained and will continue out to a radius at which the pressure of the hot gas has fallen to the same magnitude as the general gas pressure. We first discuss this central expansion.

a) Preshock Flow

The gas becomes supersonic when its pressure has decreased to $\sim P_e/2$, and it becomes highly supersonic within a few r_e. The equations then describing steady nonrelativistic expansion of an adiabatic gas can be integrated to give Bernoulli's equation, mass conservation, and an adiabatic law:

$$V^2 + \frac{2\gamma}{\gamma - 1}\frac{p}{\rho} = U^2 \tag{1}$$

$$r^2 \rho V = \frac{\dot{M}}{4\pi}, \tag{2}$$

$$p = K\rho^{\gamma}, \tag{3}$$

where V, ρ, and p are the velocity, density, and pressure

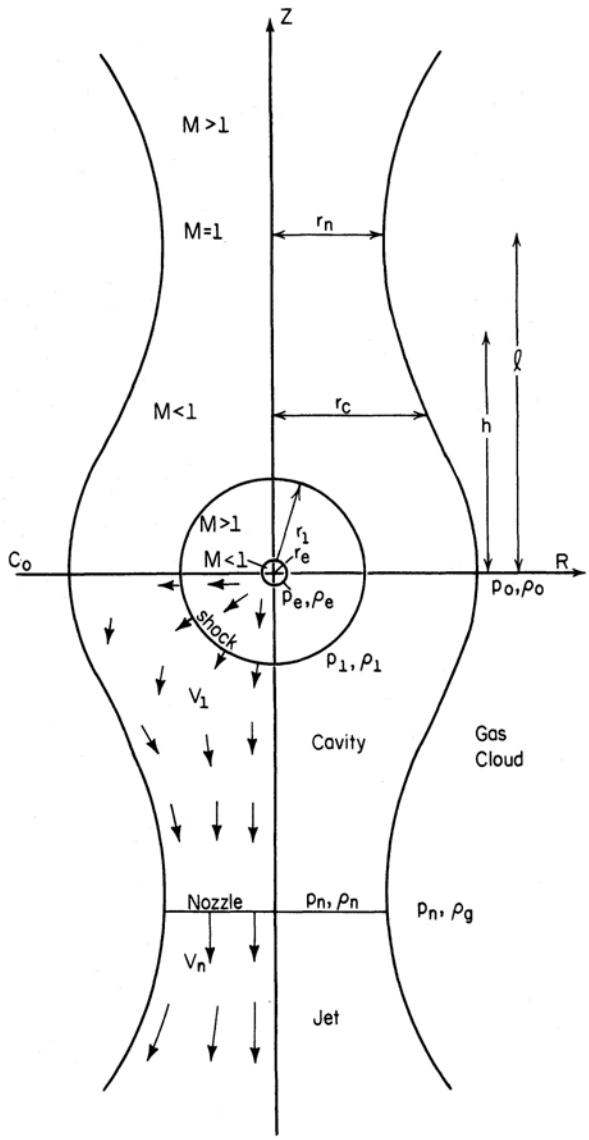


FIG. 1.—The key features of the flows we find in a cavity-nozzle structure. Definitions of the quantities are given in the text.

© American Astronomical Society • Provided by the NASA Astrophysics Data System

1983ApJ...264..432S

in the hot gas, γ is the specific heat ratio, and U, M, and K are constants. This set of equations is equivalent to the one-dimensional flow of a fluid in a jet of radius r (Smith and Norman 1981), although here V is parallel to r. At large enough r ($\gg r_e$), $p \ll p_e$, we have the approximate solutions

$$p \propto r^{-2\gamma}, \qquad \rho \propto r^{-2}, \quad \text{and } V^2 \approx \frac{p_e}{\rho_e}. \tag{4}$$

Thus, the pressure of the hot gas falls off with increasing radius out to a radius at which approximate pressure balance with the external cloud is attained.

If $p_m \propto r^{-m}$ where $m > 2\gamma$, then obviously pressure balance is never reached—the expansion remains unimpeded and simply drives out the cloud. Here, we are not interested in this extreme case and shall confine ourselves to the more probable case, $m < 2\gamma$. Then, at some radius, p approaches p_m, and the continuous flow solution will break down. A stationary shock is set up.

b) *The Central Shock*

For a nonradiative strong shock, the pressure ratio across the shock is $[2/(\gamma+1)](\rho V^2/p)$. Hence, given the external pressure distribution, p_m, and the central engine parameters p_e, ρ_e, and r_e, it is possible to determine the radius of the shock, r_1. Here, we wish to determine the parameters of the subsonic, aftershock fluid, since it is this slow moving fluid that corresponds to the "stationary" power source of the radio source model as described by Blandford and Rees (1974). At r_1 this gas has radial outflow velocity $V_1 = [(\gamma - 1)/2\gamma]^{1/2} C_1$, where C_1 is the sound speed of the shocked gas ($C_1^2 = \gamma p_1/\rho_1$). For $\gamma = 5/3$, $V_1 = 0.45\ C_1$.

To determine if the shock and preshock flow is indeed spherically symmetric, we suppose the external gas pressure to be of the form $p_m \propto a_1 R^{-m} + a_2 Z^{-m}$, with a_1, a_2, and m given constants. Since $p \propto r^{-2\gamma}$ for the preshock flow and the pressure ratio across the shock is $p_1/p \propto r^{2(\gamma-1)}$, we can calculate the distance in each direction at which pressure balance of the shocked and external gas is achieved. Consequently, we find a measure of the departure from sphericity as the shock axial ratio:

$$\frac{r_1}{r_2} = \left(\frac{a_2}{a_1}\right)^{1/(2-m)}. \tag{5}$$

Now, at the center of a potential well of a flat-bottomed potential, m will be close to zero, and so an axial pressure ratio in the surrounding cloud of R_1/Z_1 [i.e., $p_m(r = R_1, Z = 0) = p_m(R = 0, Z = Z_1)$], results in a shock axial ratio of $r_1/r_2 = (Z_1/R_1)^{m/(2-m)} \sim 1$. In a gas cloud supported gravitationally by an extended mass distribution, such as proposed by Blandford and Rees (1974), such flat-bottomed potentials are obtained. In this case the shock wave can be taken as spherically symmetric. This is in agreement with the computational results of Norman *et al.* (1981). Obviously, through these calculations we can only estimate the nature of the flow. We have implicitly assumed that a steady flow exists and that there is an outlet for the hot gas. Norman *et al.* (1981) have demonstrated that quasi-steady flows exist and the hot gas is removed from the central cavity through jets or fluid dynamic instabilities. (Here, we have assumed a steady flow out to a stationary shock front and then attempt to calculate the fate of the shocked gas. In reality the flow near r_e is highly variable. These variations are assumed to be smoothed out by $r \gg r_e$.)

We can now see that in some circumstances the scenario presented above will be invalid. If we consider a rotationally flattened gas cloud supported thermally against the gravitational field of a point mass at its center, then the initial expansion is nonspherical since m is large. Furthermore, if we consider the gas cloud to be adiabatic such that $p_m \propto \rho^\gamma$ throughout, then $p_m \propto r^{-m}$ where $m = \gamma/(\gamma - 1)$. Then for $\gamma \leqslant 2$, $m \geqslant 2$, and a stationary shock cannot form. This is caused by the dynamic pressure of the supersonic gas, $\rho v^2 \propto r^{-2}$, not being able to come into equilibrium with the gas cloud at any radius. Many possible contributing processes arise when we attempt to apply the model to galactic nuclei, e.g. radiation pressure. Thus, we are not proposing to abandon the point-mass potential since some of these processes may significantly modify the pressure distribution in the gas cloud. Blandford and Rees (1974) noted that the cavity is also more likely to be stable to homologous perturbations for $n < 2$.

c) *Postshock Flow*

The rate of mass and energy flow from the shock front surface of radius r_1 are

$$\dot{M} = 4\pi r_1^2 \rho_1 V_1, \tag{6}$$

$$L = \frac{(\gamma+1)^2}{\gamma - 1} \pi r_1^2 p_1 V_1, \tag{7}$$

where $V_1^2 = [(\gamma - 1)/2]\, p_1/\rho_1$. This subsonic hot gas inflates a cavity within the denser gas cloud. The interface is (Rayleigh-Taylor) unstable since gravity acts to push the denser gas into the cavity.

When is the Rayleigh-Taylor instability capable of removing the cavity gas? If the gas cloud were spherical, then the cavity of hot gas would grow in size until the instability is sufficient to remove hot gas from the cavity at the rate at which it is being injected. The structural effect of this instability is clearly shown in numerical simulations—the heavy fluid displaces the light fluid by

© American Astronomical Society • Provided by the NASA Astrophysics Data System

1983ApJ...264..432S

cutting under the wall and so releasing a bubble of light fluid. Although segments of light fluid are chopped off, the heavy fluid remains intact. The fragmentation time calculated by Blake (1972) is $t_{RT} \sim (2d/l_1)^{1/2}(r_c/C_g)$, where d is the size of the fragment, r_c is the cavity radius, and C_g is the sound speed in the gas cloud. This leads us to a maximum rate at which mass can be released in the form of bubbles, $\dot{M}_B \sim \pi/6 r_c^2 \rho_1 C_g$. By comparison with equation (6), we obtain an average radius for the quasi-steady flow of $r_c \sim 3.3\ r_1(C_1/C_g)^{1/2}$, where C_1 is the sound speed in the hot gas ($\gamma = 5/3$). If the cavity were smaller, then the mass injection would be greater than the mass ejection and the radius would increase, and vice versa. From this we also calculate the time a fluid element will spend in the cavity to be $t_c \sim r_c^3/3r_1^2V_1$.

A second gas escape route can be found if the cloud is not spherical. The numerical simulations (Norman *et al.* 1981) have shown that a 2:1 axial pressure ratio results in the fluid being accelerated out along the axis of greatest pressure gradient, before it can be consumed by the Rayleigh-Taylor instability. Nonsphericity introduces two effects on the hot gas—nonspherical acceleration and a change in the cavity shape. First, consider a gas cloud with a small eccentricity, e.g., $l_2 = \eta l_1$, where $p_m(l_1,0) = p_m(0,l_2)$ and $\eta \lesssim 1$. If $p_m \propto r^{-m}$, then we have introduced a pressure gradient along the interface of $\sim m(1-\eta)p_0/l_1$. This leads to an acceleration time scale, t_a, given by

$$t_a^2 \sim \frac{1}{m(1-\eta)} \frac{l_1^2}{C_1^2}, \tag{8}$$

and so

$$\left(\frac{t_a}{t_c}\right)^2 \sim 10^{-2} \frac{1}{m(1-\eta)} \frac{\rho_1}{\rho_g}. \tag{9}$$

Taking $\eta = 0.9$, $\rho_1 = 0.1\ \rho_g$, then $t_a < t_c$ for $m > 0.01$. Hence, even for small eccentricities in the surrounding cloud, it would appear that in most circumstances the flow will be accelerated out in the direction of the greatest pressure gradient (taken to be the z-axis). The above analysis is a rough indication of the effect, since l_1 is in reality determined by the smaller of the two time scales.

d) The Nozzle

The stability of the cavity will be further discussed in § IV. We conclude that the hot gas will flow out along the positive and negative z-axis rather than escape through the cavity walls. The exact steady light fluid-gas cloud configuration is then the "twin exhaust" picture, described in its one-dimensional form by Blandford and Rees (1974); the hot gas is forced through two nozzles before expanding out of the central region in the form of two jets. This steady flow is only one possible resulting flow and is shown in Figure 1.

At the nozzle (minimum jet cross-sectional area) the flow is transonic (see Courant and Friedrichs 1948 for a complete discussion). Applying mass and energy conservation the nozzle radius, r_n, and pressure, p_m, are found to be

$$\left(\frac{r_n}{r_1}\right)^2 = 2\left(\frac{2\gamma}{\gamma+1}\right)^{1/(\gamma-1)}\left(\frac{\gamma-1}{\gamma+1}\right)^{1/2} \tag{10}$$

and

$$\frac{p_m}{p_1} = \left(\frac{\gamma+1}{2\gamma}\right)^{\gamma/(\gamma-1)}. \tag{11}$$

For $\gamma = 5/3$, $r_n = 1.18\ r_1$ and $p_m = 0.57\ p_1$. The nozzle radius is slightly larger than the central shock front radius as first recognized by R. D. Blandford (private communication) and Rees (1976). Here we have assumed a constant pressure across the nozzle, corresponding to a one-dimensional flow. A large pressure gradient across the nozzle can occur (see § III). Furthermore we have assumed the same Bernoulli constant to apply to each fluid element and the interface between the fluids to be a sharp boundary across which the pressure is continuous. These simplifying assumptions have been corroborated through the numerical work of Norman *et al.* (1981).

The nozzle height, l, is approximately given by the external pressure scale height. To completely specify the cavity dimensions we proceed to find a relation between r_n and l. The jets' luminosity can be written

$$L_j = \gamma \frac{\gamma+1}{\gamma-1} \pi r_n^2 p_n V_n. \tag{12}$$

We can also form a quantity with the dimensions of luminosity from the parameters describing the gas cloud, $L_m = p_n C_g l^2$. Then

$$\frac{L_j}{L_m} \sim \pi\gamma \frac{\gamma+1}{\gamma-1}\left(\frac{\rho_g}{\rho_n}\right)^{1/2}\left(\frac{r_n}{l}\right)^2, \tag{13}$$

where ρ_n/ρ_g is the density ratio between the jet and cloud (for simplicity we take a specific heat ratio ~ 1 for the cloud). In this terminology, the dimensionless luminosity is given by the density and r_n/l ratios. These two ratios will be of great significance in the stability analysis of the following sections. Since the ratio r_n/r_1 is specified we are able to estimate the response of the central source to changes in the environment. Consequently, we hope to determine the range of L_j/L_m for which jets are stable.

© American Astronomical Society • Provided by the NASA Astrophysics Data System

1983ApJ...264..432S

III. NOZZLE STABILITY

It has long been thought that instabilities at the nozzle have the potential to destroy the jet flow (Scheuer 1974; Turland and Scheuer 1976; Blandford and Pringle 1976; Blandford 1978). This is a consequence of the one-dimensional approximations made previously, resulting in a long thin nozzle along which instabilities can be very disruptive. Here we examine the most serious fluid dynamic instability that acts across on interface separating fluids in relative motion. This is the Kelvin-Helmholtz instability and is here applied to the jet-gas cloud interface at the nozzle.

First, we shall demonstrate the disruptive ability of the instability by taking the incompressible fluid phase speed, V_p, and growth rate, Γ, for a small sinusoidal disturbance of frequency ω and wavenumber k propagating on the interface at an angle ϕ to the flow direction in the jet (e.g., Blake 1972):

$$V_p = \frac{\rho_n}{\rho_n + \rho_g} V_n \cos\phi, \tag{14}$$

$$\Gamma = \frac{(\rho_n \rho_g)^{1/2}}{\rho_n + \rho_g} V_n \cos\phi. \tag{15}$$

The time elapsed, τ_{KH}, before the wave enters the nonlinear region, with amplitude $1/k$, is dependent on the amplitude of the initial disturbance. Since the growth rate is exponential, we can take $\tau_{KH} \sim 3/\Gamma$. Similarly, the relevant convection scale length is the height through which the nozzle remains relatively thin, here taken as $\sim l$. Using equations (14) and (15) we obtain the ratio

$$\tau_{KH}/\tau_C \sim \frac{3}{2\pi}\left(\frac{\rho_n}{\rho_g}\right)^{1/2}\frac{\lambda}{l}, \tag{16}$$

where $\tau_C = l/V_p$ is the disturbance convection time, and wavelength $\lambda = 2\pi/k$. Since $\rho_n < \rho_g$, we have $\tau_{KH} < \tau_C$, and we cannot resort to convection as a stabilizing influence. For simplicity, the instability rates analyzed in this section are those occurring on a plane interface ignoring the cylindrical nature of the problem. These results are accurate for small wavelength disturbances, for which the growth rate is largest.

We shall follow the discussion of the nonlinear stage of the instability given by Blake (1972), i.e. a boundary layer of increasing thickness moves into the jet with velocity

$$V \sim \frac{(\rho_n \rho_g)^{1/2}}{\rho_n + \rho_g} V_n. \tag{17}$$

The jet will then be cut off in a time estimated to be r_n/V, and a bubble of hot gas is disconnected from the central source. In this manner a series of bubbles is formed. (These are not the bubbles attained by Gull and Northover 1973 for which buoyant hot gas is chopped off through long wavelength Rayleigh-Taylor instability modes in the central cavity.)

In the numerical simulations of Wiita (1978*b*) and Norman *et al.* (1981) the bubbles only result for small luminosities corresponding to small nozzle radii in the steady jet solution, equation (13). Hence, we believe the above analysis to be incomplete and we shall go on to consider the effects of (1) compressibility, (2) pressure gradients across the nozzle (§ IV), and (3) the extraction of momentum from the jet.

We shall now consider the compressible fluid dispersion relation and derive relevant growth rates to compare with the incompressible case discussed above. While the finite sound speed tends to stabilize the jet just after the nozzle, we shall see that at the nozzle itself growth rates are enhanced. We again investigate the plane interface problem (cylindrically symmetric jets have been investigated by Ferrari, Trussoni, and Zaninetti 1978 and Hardee 1979). The dispersion relation in its simplest form for compressible fluids is given by Pai (1954):

$$\frac{\sigma_1}{\gamma_1(1-\sigma_1^2)} = -\frac{\sigma_2}{\gamma_2(1-\sigma_2^2)}, \tag{18}$$

where the suffixes 1 and 2 are used in this scenario to refer to the jet and gas cloud, respectively, and

$$\sigma_1^2 \equiv 1 - \left(\frac{\omega - k_z V_1}{kC_1}\right)^2 \equiv 1 - M_1^2, \tag{19a}$$

$$\sigma_2^2 \equiv 1 - \left(\frac{\omega}{kC_2}\right)^2 \equiv 1 - M_2^2. \tag{19b}$$

Here, $k_z = k\cos\phi$, where ϕ is the angle between k and V_1. Here we shall take both fluids to be nonrelativistic with $\gamma_1 = \gamma_2 = 5/3$. Unequal ratios of specific heat ratios have been discussed by Blandford and Pringle (1976) for certain limiting cases.

From equation (18) we can derive a condition for stability (Fejer and Miles 1963):

$$M_c \cos\phi \equiv \frac{V_1}{C_1}\cos\phi > \left[1 + \left(\frac{\rho_1}{\rho_2}\right)^{1/3}\right]^{3/2}. \tag{20}$$

Consequently, at the nozzle ($V_1 = C_1$) the flow is unstable, although the flow parameters are close to the stability regime. We shall look for solutions to equation (18) at the nozzle to determine how the growth rate and phase speed are effected.

© American Astronomical Society • Provided by the NASA Astrophysics Data System

1983ApJ...264..432S

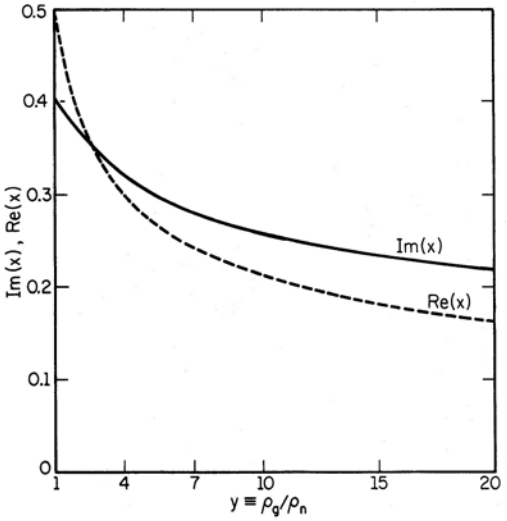


FIG. 2.—The phase speed Re(x) (in units of C_1) and the growth rate Im(x) (in units of kC_1) for Kelvin-Helmholtz instability at the nozzle are given as a function of density ratio.

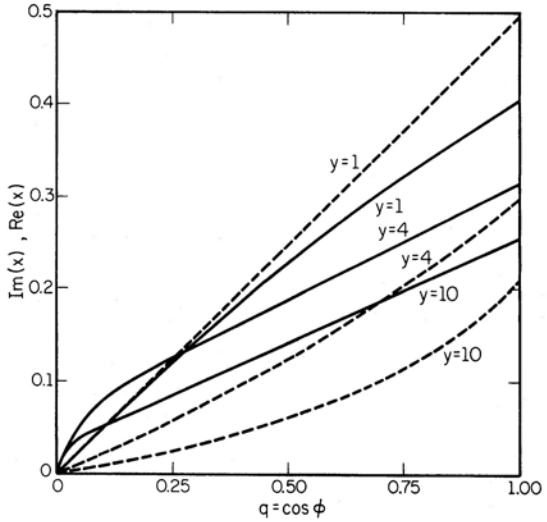


FIG. 3.—The same quantities as Fig. 2 plotted vs. the angle ϕ between the flow speed and the wave vector for various values of density ratio.

Writing $x = \omega/kC_1$, $q = \cos\phi$, and $y = \rho_2/\rho_1 = C_1^2/C_2^2$, we obtain

$$x^4 j - 2qx^3 y + \left[(q^2-1)y - 1\right]x^2 + 2qx - q^2 = 0. \tag{21}$$

The root corresponding to the unstable Kelvin-Helmholtz mode is easily found after q and y are specified. In Figure 2 the phase speed (in units of C_1) and growth rate (in units of kC_1) is given as a function of the density ratio. Figure 3 demonstrates the variation in the growth rate for various values of ϕ.

From equation (18) we find that, as $\rho_2/\rho_1 \to \infty$ and with $\phi = 0$,

$$\frac{\omega}{kC_1} \approx 2^{-4/3}(1 \pm i\sqrt{3})\left(\frac{\gamma_1}{\gamma_2}\right)^{1/3}\left(\frac{\rho_1}{\rho_2}\right)^{1/3}. \tag{22}$$

Hence, the presumption made above of $\gamma_1 = \gamma_2$ provides a good estimate to the instability at the nozzle.

An interesting example to take is $y = 4$, corresponding to the density ratio at the nozzle in the hydrodynamic model (Norman *et al.* 1981). We note that the simulations were cylindrically symmetric and so give modes with $\phi = 0$, and that they result in toroidal "blobs" that break off from the interface and are then accelerated by the jet. Equation (21) has the two complex roots

$$\frac{\omega}{kC_1} \approx 0.03 \pm 0.32i. \tag{23}$$

This is in reasonable agreement with the initial phase speed of the blobs in the numerical model of $\sim 1/3C_1$. Consequently, the numerically determined instability appears to closely resemble the nature of a more general type of disturbance.

We conclude that the growth rates are not significantly changed from the incompressible values; however, some interesting results are apparent. Despite the proximity to the critical Mach number M_c, growth rates are enhanced. Small wavelength modes grow fastest and become nonlinear in a time $\sim 0(1/\omega)$ in which the disturbance has moved a distance $\sim 0(q/k)$ along the jet, with little dependence on the density ratio. Here we take the view that the small wavelength perturbations dominate to the point of saturating the surface and inhibiting the growth of large scale disturbances (this will justify the use of the plane flow approximation to the cylindrical flow). This conforms to the numerical calculations where it was demonstrated that the surface at the nozzle becomes ragged and blobs are released on the minimum scale admitted by the grid size.

The maintenance of the jet will depend on the capability of the instability to extract momentum therefrom. If the jet thrust is large enough, then the instability is unlikely to bring the whole jet to a halt, whereas if the nozzle region is long and thin, then the vortex boundary layer can destroy the jet flow. We calculate the effect in the following simplified manner. A growing disturbance of wavelength λ will extract momentum $\sim \pi/48\rho_g V_p \lambda^3$ from the jet in a time $\sim (3\lambda/2\pi V_n)[1/\mathrm{Im}(x)]$. Since there is space for $\sim 8r_n l/m\lambda^2$ such disturbances, the total momentum absorbed by the gas cloud per unit time is $\sim \mathrm{Re}(x)\times\mathrm{Im}(x)(\rho_g/\rho_n)(r_n l/m)\rho_j V_n^2$.

© American Astronomical Society • Provided by the NASA Astrophysics Data System

1983ApJ...264..432S

The momentum flow rate (thrust) of a jet is $\sim \pi r_n^2 \rho_j C_j^2$. Comparison of the two forces yields a critical nozzle radius such that the jet is maintained for

$$\frac{r_n}{l} \gtrsim \frac{r_{\min}}{l} \sim \frac{1}{3m}\mathrm{Re}(x)\times\mathrm{Im}(x)\left(\frac{\rho_g}{\rho_n}\right). \quad (24)$$

As an example we take $m = 0.7$ and the solution to the dispersion relation for $\rho_g = 4\rho_j$. We obtain $r_c = 0.18l$, a critical radius that agrees with the numerical simulations of Norman *et al.* (1981).

The minimum radius is dependent on the density ratio and takes on values between $0.07/m$ and $0.15/m$ for density ratios between 1 and 10. For higher density ratios the nozzle radius becomes comparable with the nozzle height. That is, higher external densities are more efficient in nozzle degeneration.

We conclude that long thin nozzles such as previously proposed (e.g., Blandford and Rees 1974) are, in general, unstable. For $\rho_j \gtrsim 0.1\rho_g$, we expect to be able to maintain the jet for $r \gtrsim 0.1l$ provided m is not close to zero. That is, short stubby nozzle geometries are stable. Substituting equation (24) into equation (13) we obtain the minimum double jet luminosity, $L_{\min}$:

$$\frac{L_{\min}}{L_m} \sim \frac{\gamma(\gamma+1)}{3(\gamma-1)}\left(\frac{1}{m}\right)^2[\mathrm{Re}(x)\times\mathrm{Im}(x)]^2\left(\frac{\rho_g}{\rho_n}\right)^{5/2}. \quad (25)$$

$L_{\min}$ is dependent upon the parameters describing the gas cloud and the density ratio across the nozzle. Consequently the form of equation (25) is particularly useful for applications.

IV. JET CHOKING

a) *Rayleigh-Taylor Instability*

The remaining stability problem needing attention is that of the central cavity. Here we have a hot gas in a cavity, supporting surrounding cooler and denser gas. In such a situation the cavity walls are unstable with the gravitational acceleration, g, forcing cool gas into the cavity. This is the Rayleigh-Taylor instability which can also be combined with the Kelvin-Helmholtz instability if there is a relative flow across the cavity wall. The dispersion relation (Blake 1972) leads to a fragmentation time

$$\tau_{\mathrm{RT}} \sim \left[\frac{2\pi\rho_2(\rho_1+\rho_2)l}{\xi\rho_1(\rho_2-\rho_1)kC_j^2}\right]^{1/2} \quad \text{and}$$

$$\left(\frac{\tau_{\mathrm{RT}}}{\tau_{\mathrm{KH}}}\right)^2 \sim \frac{1}{\xi}\frac{\rho_2^2}{\rho_2^2-\rho_1^2}\left(\frac{V_1\cos\phi}{C_j}\right)^2 kl. \quad (26)$$

Here, we have related g to the gas cloud parameters by $g = C_g^2/l = \xi(\rho_j C_j^2/\rho_g l)$. Then, for $\xi \sim 1$, the gas cloud is thermally supported against gravity (if $\xi \lesssim 1$ the gas is not bound to the cavity region unless other physical processes are effectively containing the gas cloud. If $\xi > 1$ then the gas cloud must be supported against gravity by some further mechanism). Here, $g \equiv GM(l)/l^2$, where $M(l)$ is the total mass (of gas and compact objects) within a sphere of radius l. We have also taken $\phi = 0$, corresponding to gravitational acceleration perpendicular to the cavity wall.

From equation (26) we deduce that the Rayleigh-Taylor instability is dominant for large scale disturbances where $V_1^2 < C_j^2 k$. Thus, large chunks of slow moving hot gas can be released into the major plane of the flattened gas cloud before being convected away from the plane. This is seen in the numerical simulations of Norman *et al.* (1981), where we can also see how the instability proceeds in the nonlinear regime: the heavy fluid displaces the light fluid by "cutting under" the wall so as to chop off a cloud of hot gas (see § VI). Small scale disturbances grow most effectively through the Kelvin-Helmholtz instability. As these disturbances grow, they are also convected towards the nozzle. Since convention has already been shown to be ineffective, the maximum amount of hot gas that can be released through the walls by these instabilities is $O(\rho_1 C_g r_c l)$ per unit time, where r_c represents an average cavity radius. This is a fraction $O(r_c l C_g/r_n^2 C_j)$ of the mass flow rate. Thus the efficiency of mass transfer will largely depend on the cavity radius. The exact cavity shape and the response of the inner shock front to external disturbances must be determined for an accurate analysis. The second factor is complex and will not be considered here, since no obvious effect of this kind is apparent from the numerical simulations.

b) *Cavity Structure*

An average cavity radius, r_c, can be obtained if we simplify the flow within the cavity. While the instability is not destructive, we shall demonstrate that the overall flow pattern is not in equilibrium as $r_n/l \to 0(1)$.

The cavity volume, $\sim 2\pi r_c^2 l$, can be divided into two parts (see Fig. 1), one being the volume, $4/3\pi r_1^3$, within the central shock. If $\hat{\rho}$ is the average density within the subsonic region, then

$$\hat{\rho}\left(2\pi r_c^2 l - 4/3\pi r_1^3\right) = 2\pi r_n^2 \rho_n V_n t, \quad (27)$$

where the right-hand side is the mass contained in the subsonic region determined by the average time, t, a gas element requires to reach the nozzle from the shock front. We can take $\rho_n \sim 0.9\hat{\rho}$, $r_n \sim 1.18 r_1$, and we find

$$t \sim \left[\left\{(l-1/2r_1)^2 + 1/2\left[\left(r_c^2+3/4r_1^2\right)^{1/2} - r_n\right]^2\right\}^{1/2}\right]\hat{V}^{-1}, \quad (28)$$

© American Astronomical Society • Provided by the NASA Astrophysics Data System

1983ApJ...264..432S

where $\hat{V} \sim 1/2(V_1 + V_n) \sim 0.63V_n$. The first term for t inside the brackets is the average distance traveled along the z-axis, and the second term is an average distance traveled perpendicular to the z-axis. This yields $1.7 < (r_c/r_1)^2 < 1.9$ for $0 < r_1/l < 1$, and the mass lost through the cavity boundary is small. The result obtained here, that r_c is roughly proportional to r_1, is in concurrence with the numerical simulations. Finite speed of sound effects when $r_n = 0(l)$ and mass loss through the Rayleigh-Taylor instability are contributing factors that have not been taken into account.

The most significant factor to appear here is the change in the nature of the flow when the cavity-nozzle structure becomes stumplike. As $r_n \to 0(l)$ the pressure difference across the nozzle becomes equal to the pressure difference between the nozzle and central shock. The flow is then no longer of the de Laval nozzle form and, as will now be shown, cannot be in equilibrium. For a stationary flow, the pressure gradient perpendicular to the symmetry axis must balance the centrifugal force of the flow through the nozzle. The latter force, $\rho_n V_n^2/R$, is determined by the radius of curvature, R, of the nozzle walls (in a plane containing the z-axis). Given the radius r_c at a distance $1/2l$ from the nozzle, $R \sim 1/8l[l/(r_c - r_n)] + 1/2(r_c - r_n)$. We thus estimate that for $r_n \sim 0.7l$ the nozzle pressure on the z-axis will be $\sim p_1$, the central shock pressure. Therefore, additional flow toward the nozzle is stopped, bloating out the central cavity. Continued outflow through the nozzles only intensifies the nonequilibrium situation. Finally, when a nozzle radius small enough to be supported by a small pressure difference (but high gradient) is reached, the nozzle is Kelvin-Helmholtz unstable. The conclusion is that recurrent nozzle choking will take place with large clouds of slow-moving light gas being ejected along the symmetry axis between choking. The cavity radius also oscillates (see § VIII); when the nozzle is choked and the cavity expands, a number of smaller clouds will be released in all directions through the Rayleigh-Taylor instability. From Equation (15), the maximum twin jet luminosity, corresponding to $r_n \lesssim 0.7l$, is

$$\frac{L_{\max}}{L_m} \sim 0.5\pi\gamma\frac{\gamma+1}{\gamma-1}\left(\frac{\rho_g}{\rho_n}\right)^{1/2}. \quad (29)$$

The implications of the existence of an upper limit will be explored in § VI.

V. INTERPRETATION

In previous sections we have probed cavity-jet structures and obtained upper and lower limits on the power of a central source for which jets can be sustained. Consistency with numerical simulations has been achieved. The analytical formalism now leads us to a deeper understanding and detailed interpretation of the results. In this section diverse problems that must precede direct astrophysical applications are discussed.

a) *Eccentricity*

The eccentricity of the gas cloud leads to a nonspherical central shock within the cavity of hot gas. In § II we determined that this is important for high eccentricities in which the pressure decreases with radius as a power law with index $m > 1$. A further complication with such clouds is the lack of a clearly defined scale height, h, to which the nozzle height, l, can be related. The nature of these difficulties is brought out by first considering a cloud in which thermal pressure supports the gravitational attraction of a uniform stellar distribution. Such clouds, reviewed by Wiita (1978*a*), can derive their eccentricity through either an oblate spheroidal potential or rotation. Here, a well-defined scale height is given by $h^2 = kT/\pi G\rho_s m_p$, where T is the cloud temperature and ρ_s is the stellar mass density. This leads to a flat-bottomed pressure distribution almost indistinguishable within the cavity from that utilized in the numerical simulations of Norman *et al.* (1981):

$$p(R, Z) = p_0 \exp\left[\left(-A_1R^2 - A_3Z^2\right)/(2h^2)\right] \quad (30)$$

with $2A_1 + A_3 = 2$, and the cloud eccentricity $e^2 = 1 - A_1/A_3$. Using this pressure, simple calculations gives deviations from spherical symmetry of $Z_1/r_1 \sim 1$–1.42 for a cloud with a 2:1 axial pressure ratio. The ratio increases with cavity size and corresponds closely to that measured from the numerical simulations 1–1.33. Thus the approximate sphericity assumed in previous sections is a reasonable estimate for our purposes.

b) *Luminosity Range*

Given the cloud, the values of the parameters of the central engine then characterize the flow completely. The high pressure gas released from this source may come into equilibrium with the gas cloud within the flat-bottomed region of the Gaussian distribution, i.e., $p_1 \sim p_0$. As the central pressure is increased, however, this does not remain true, and we must determine the distance at which pressure balance is achieved. Consequently, the nozzle height l is not fixed. Hence, to determine a luminosity range, we make use of the fixed scale height h to define a dimensionless luminosity by $\mathfrak{L} = L/(P_0C_0h^2)$, where C_0 is the central gas sound speed. The nozzle height and L/Lm are related to h and $\mathfrak{L}$ by the cloud eccentricity and cavity size.

As an example, we shall fix the sound speed of gas ejected from a central engine of fixed radius, i.e., p_e/ρ_e is constant, but allow its power to take all values. It follows that C_1 is a constant and the nature of the flow—either jets, clouds, or bubbles—is determined by L, C_1/C_0, and e through equations (25), (29), and (30).

© American Astronomical Society • Provided by the NASA Astrophysics Data System

1983ApJ...264..432S

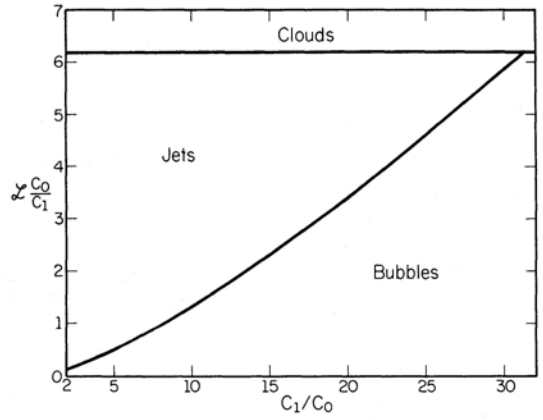


FIG. 4.—The three regimes of the global hydrodynamic behavior are separated out by plotting the luminosity vs. the sound speed ratio.

In this manner we have obtained Figure 4 for $e = 0.87$, and Figure 5 for $C_1/C_0 = 10$. We have plotted $\mathcal{L}C_0/C_1$ to provide a simpler visual representation.

Figure 4 demonstrates a remarkable result. If the sound speed of the hot gas is greater than 30 times the sound speed of the confining cloud, it is impossible to form jets! This corresponds to a cloud-to-cavity density ratio of greater than 10^3. Furthermore, for buoyancy forces to be present, the cloud must be the denser, i.e. $C_1 > C_0$. Since the dynamics of the cloud become of importance for $C_1 \lesssim 2C_0$, we have limited our results to $C_1 > 2C_0$. The main conclusion to be drawn from Figure 4 is that jet luminosity ranges of greater than one magnitude occur only for $C_1 < 5.5C_0$, or cloud-to-cavity density ratios < 30.

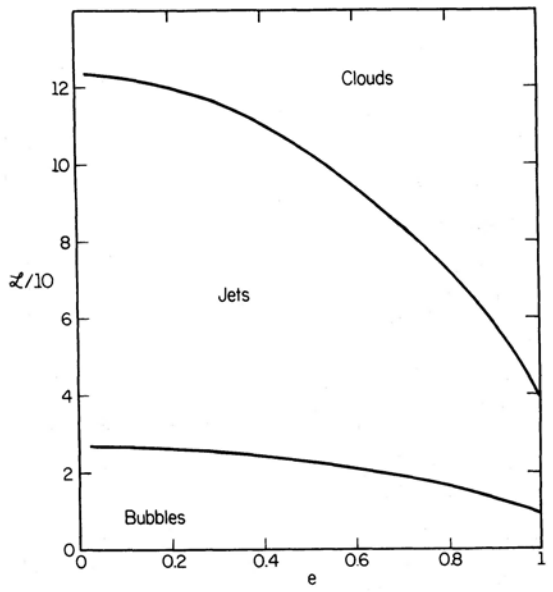


FIG. 5.—The luminosity ranges as determined by the eccentricity e of the confining cloud.

Eccentricity has little effect on the luminosity range. Higher eccentricities lead to lower luminosities, due to the decrease in the pressure scale height along the jet axis. As expected, these results are distinct from those obtained by Wiita (1978*b*), where a relativistic gas was considered, and many simplifying assumptions were made. However, they are in rough agreement with the more sophisticated numerical results (Norman *et al.* 1981). Corresponding to $\rho_g \sim 5\rho_n$, their maximum jet luminosity is a factor of 2 greater, and the minimum is a factor of 4 greater. These factors are insignificant, considering the methods employed, and the limitation to axisymmetric disturbances in the numerical study.

VI. ASTROPHYSICAL IMPLICATIONS

We shall now convert our results into forms useful for application to radio galaxies. We will confine ourselves to nonrelativistic jets formed in a flat-bottomed potential well. The constraints on quasars and other sources requiring relativistic motions will be analyzed elsewhere.

a) Mass of Galactic Nucleus

First, we relate the cloud sound speed to the total mass M_t contained within a radius h by $\xi C_0^2 = GM_t/h$. By also using $p_0 = \gamma\rho_0 C_0^2 = (3\gamma/4\pi h^3) M_g C_0^2$, where M_g is the mass of the gas cloud within a radius h, the jet luminosity maximum can be written

$$\left(\frac{L_{\max}}{10^{46}\ \mathrm{ergs\ s^{-1}}}\right) = 1.0\xi\left(\frac{C_1}{3C_0}\right)\left(\frac{10^7 M_g}{M_t}\right)\left(\frac{C_0}{10^4\ \mathrm{km\ s^{-1}}}\right)^5; \tag{31}$$

the jet luminosity minimum is

$$\frac{L_{\min}}{10^{46}\ \mathrm{ergs\ s^{-1}}} = 0.07\xi\left(\frac{C_1}{3C_0}\right)^{7/3}\left(\frac{10^7 M_g}{M_t}\right) \times\left(\frac{C_0}{10^4\ \mathrm{km\ s^{-1}}}\right)^5, \tag{32}$$

and the cloud radius (presuming an eccentricity $e \gtrsim 0$) is

$$\left(\frac{h}{0.01\ \mathrm{pc}}\right) = 0.7\xi^{-1}\left(\frac{M_t}{10^8 M_\odot}\right)\left(\frac{C_0}{10^4\ \mathrm{km\ s^{-1}}}\right)^{-2}. \tag{33}$$

We have used numbers that may correspond to a powerful radio galaxy such as Cygnus A. Thus, jet luminosities are critically dependent on M_g/M_t and C_0, or M_g/M_t, M_t, and h. For the more typical radio galaxy the central

© American Astronomical Society • Provided by the NASA Astrophysics Data System

1983ApJ...264..432S

cloud may be much more extensive, in which case we can use

$$\left(\frac{L_{\max}}{10^{43}\ \mathrm{ergs\ s^{-1}}}\right) = 1.0\xi\left(\frac{C_1}{3C_0}\right)\left(\frac{10^5 M_g}{M_t}\right) \times \left(\frac{C_0}{10^3\ \mathrm{km\ s^{-1}}}\right)^5, \quad (34)$$

$$\left(\frac{h}{100\mathrm{pc}}\right) = 0.7\xi^{-1}\left(\frac{M_t}{10^{10}M_\odot}\right)\left(\frac{C_0}{10^3\ \mathrm{km\ s^{-1}}}\right)^{-2}. \quad (35)$$

Besides observational limits on h, a second cloud constraint is derived from the free-free electron emission process in the X-ray range. This was first considered by Blandford and Rees (1974) in the original relativistic thin jet model that required $l \gtrsim 2r_c \gtrsim 10r_n$. For Cygnus A, a jet luminosity of $\gtrsim 10^{46}$ ergs s^{-1} is required, and an upper limit to the X-rays is $\sim 2\times10^{45}$ ergs s^{-1}. They proposed $l \lesssim 100$ pc, $T_0 \sim 3\times10^8$ K and $M_t \sim 10^4\ M_\odot$ pc^{-3}, thus satisfying the further constraint of a stellar mass $\lesssim 10^{10}\ M_\odot$ within this distance of the center of giant ellipticals. Later, Wiita (1978*a*) used VLBI results that indicated a nucleus of at most a few parsecs to demonstrate that a consistent set of parameters is: $h =$ 0.96 pc, $T_0 \sim 2.1\times10^9$ K, $\rho_0 \sim 0.16$ dyn cm^{-2}, and masses are $M_t \sim 5.2\times10^9\ M_\odot$ and $M_g \sim 2.3\times10^4\ M_\odot$.

We can now see the advantages of the cavity and nozzle structures developed in this paper. Taking these parameters ($\xi = 1.1$) and a cavity sound speed $C_1 \sim 5C_0 \sim 0.1C$ (i.e., relativistic corrections can be ignored), a wide luminosity range is obtained: $L_{\min} = 8.6\times10^{45}$ ergs s^{-1} and $L_{\max} = 1.1\times10^{47}$ ergs s^{-1}.

A full interpretation of these results for sources with jets will be discussed by Smith *et al.* (1981). Here we shall concentrate on the optically thin model for Cygnus A, since this is one of the most powerful and well observed radio galaxies. A consistent set of parameters are: $M_t \sim 10^9$–$10^{10}\ M_\odot$, $M_g \sim 10^2$–$10^4\ M_\odot$, $C_0 \sim (6\times10^3)$–10^4 km s^{-1}, and $(\dot{M}) \sim 10$–$30\ M_\odot$ yr^{-1}. This gives a central pressure of $P_0 \sim 1$–10 dyn cm^{-2} and indicates that the thermal gas energetically dominates within 1 pc (see Kafatos 1978). The latest VLBI maps show that a jet on this scale exists (Linfield 1981).

b) *The Power-Temperature Relation*

One of the most interesting results to explore is the high dependence of the jet power on the temperature of the central cloud. Although there is great uncertainty in the mass ratio M_g/M_t, a dominant relation of the form $L \propto T^{5/2}$ may be indirectly observable. This is deduced from the several orders of magnitude (between 10^{39} and 10^{48} ergs s^{-1}) in radiated power from extended sources. Here this range is explained by a relatively small range in central temperatures of between 10^6 and 10^9 K. If this is so, then we can look for ways in which the relationship would be observed.

A correlation between monochromatic radio luminosity and the optical magnitude of the underlying galaxy was found by Auriemma *et al.* (1977) for radio galaxies. While the extended radio luminosity will undoubtedly be related to the jet power, it is difficult to conceive a relationship between the optical magnitude on the scale of tens of kiloparsecs and the central cloud temperature on the scale of less than a parsec. However, the underlying galaxy can influence the central engine if it mediates in the supply of fuel. This extra factor will be dealt with in a later paper.

The extended radio power, P_e, of radio quasars appears to be related to the core radio power, P_c. The suggested relation is $P_e \propto P_c^2$ (Miley 1980). A similar type of relation probably exists for radio galaxies (Miley 1980). The weakness of core components inhibits a more definite statement, and, moreover, since at least two types of core exist, the meaning of any relationship is complex. The above relationships are consistent with the fluid jet model if the core radio power is positively correlated with the central cloud temperature as would indeed be expected. This, of course, assumes that the extended radio emission is positively correlated with the power entering the extended lobes through the jets.

c) *A Schematic Picture*

Finally, we shall relate the central sound speed, C_0, to the width of emission lines in the various extragalactic objects. In the simplest manner, we shall equate C_0 with the mean velocity derived by assuming the emission lines are produced by a large number of filaments. This would be reasonable for a number of models of nuclei, such as free fall of filaments close to the central cloud or constant velocity outflow that was preceded by acceleration within the central cloud to $\sim C_0$. One needs to ensure that the emission spectra observed are from the compact component rather than from an extended distribution of filaments. Thus, it is usually the broad lines that are relevant since the narrow lines are produced from a much larger region (Heckman *et al.* 1981).

In sources with jets or where jets are predicted, further information on C_0 can be deduced. Thus, in a number of weak radio galaxy jets a velocity of 10^3–(3×10^3) km s^{-1} is estimated. Hence we expect $C_0 \sim 10^3$ km s^{-1}. In quasars with superluminal motions, a relativistic sound speed is necessary in most interpretations. A schematic picture is outlined in Figure 6. We have taken $\xi = 1$, $C_1 = 3C_0$, and $M_g = 10^{-6}M_t$, the latter being a hand-waving assumption. Different values of M_g/M_t, however, will push the jet band up or down the C_0-axis only as $(M_t/M_g)^{1/5}$. In the diagram we have tentatively assigned regions for each type of object. The diagram

© American Astronomical Society • Provided by the NASA Astrophysics Data System

1983ApJ...264..432S

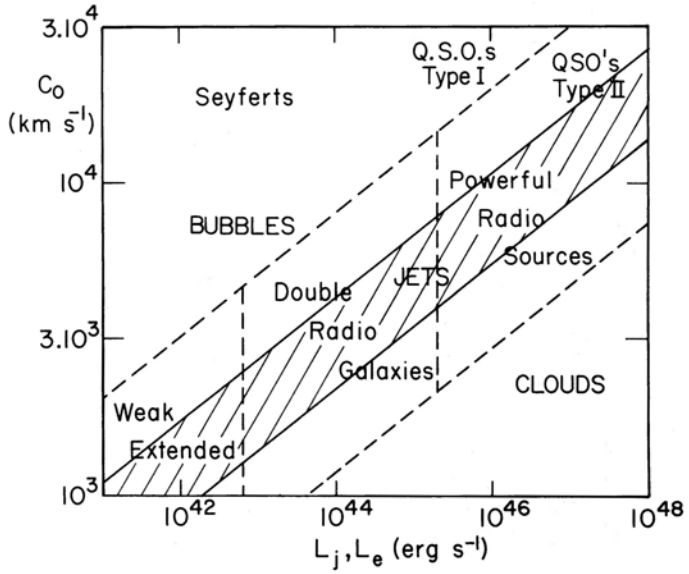


FIG. 6.—A schematic classification of active galactic nuclei suggested by our investigation

was inspired by a need for a new outlook on powerful galactic nuclei and is based on limited evidence. Notice that sources with jets overlap the jet band but are not wholly contained within. We expect nuclei to evolve across the diagram spending only a small fraction of its time ejecting material through jets. Consequently, the absence of observed jets in the majority of sources may be partially due to this effect.

We have isolated a single parameter—C_0. As to whether a source actually is jetting is dependent on the fueling and the nature of the central source. Both these factors may be physically related to C_0, making any simple interpretation impossible.

Is it possible to place other active nuclei on this diagram? To do so, we must generalize the jet power to the power ejected from the central engine, L_e. Then presume L_e is of the same order of magnitude as the total power emitted over all energy bands. We note that these sources lie in the bubble region. For sources lying close to the jet band, we expect the ejection of large bubbles of hot gas (see § VII).

No nuclei have been placed in the cloud (Rayleigh-Taylor unstable) region. We suggest that highly active central engines are efficient at heating the central cloud, thus tending to keep them above the jet-band. Source evolution from the left-hand side to the right-hand side of the diagram and back again would produce the same effect: any source in the cloud region would possess extended components.

We see no objections to this picture that cannot be overcome through combinations of evolution across the diagram, changes in M_g/M_t, etc. We leave the interested reader to determine the positions of more complex sources. Seyfert galaxies are very similar to quasars in emission spectra, and they are very similar to radio galaxies in power (giving them a unique position in the figure). It then follows that they lie well away from the jet band and resolves the fact that they do not have extended structure. Quasars seem to fall into two classes, types I and II (Ku, Helfand, and Lucy 1980). Type I quasars are radio quiet with highly luminous cores, like Seyferts galaxies, but more powerful. Type II quasars, only 10% of all quasars, often have extended radio lobes (Miley and Hartsuijker 1978). Our scheme allows for a natural separation of these types (see Fig. 6). While this picture is difficult to test rigourously, no obvious contradiction is apparent when compared to galactic nuclei.

VII. BUBBLES

A lower limit to jet powers was obtained in § III. Below the limit the nozzle is unstable. We expect a bubble to be released on the nozzle collapse time scale. After one collapse, the nozzle quickly reforms, since cavity gas is continuously accelerated towards the nozzle. Thus light gas generated by the central engine is carried out of the central cloud in a number of bubbles. Comparison of time scales in § II demonstrated that this sequence will occur as opposed to the cavity bloating out when the nozzle escape route is blocked and is consistent with numerical work done by Wiita (1978*b*) and Norman *et al.* (1981). As we shall now see, however, theoretical considerations lead us to expect vastly different emerging structures than obtained through the numerical simulations.

The disruptive force, F, and the thrust, F_T, on the nozzle were derived in § III. For $r_n < r_{\min}$ (or $L < L_{\min}$),

© American Astronomical Society • Provided by the NASA Astrophysics Data System

1983ApJ...264..432S

$F > F_T$. Replacing l/n by the length l' of the growing nozzle, we then see that $F \propto l'$ and $F \to F_T$ as $l' \to \tilde{l}$, where $\tilde{l} < l/n$ if $r_n < r_{\min}$. Hence the flow is completely disrupted beyond $\tilde{l}$. Before the nozzle has developed this far, the leading edge advances with a speed $v_b \sim (\rho_n/\rho_g)^{1/2} v_n$ along the symmetry axis. By the time the leading edge reaches $\tilde{l}$, the mass $\pi r_n^2 \rho_n v_n (\tilde{l}/v_b)$ escapes into a bubble. A similar excess of light gas around the symmetry axis during the formation of jets is seen in the numerical simulations. The leading edge of the bubble can be moving supersonically as first shown by Wiita (1978*b*). However the dense gas rapidly decelerates it to a subsonic terminal speed $\sim (r_n g)^{1/2}$, where g is the gravitational acceleration (Gull and Northover 1973).

More large bubbles will not be released because the nozzle has been evacuated. Cavity gas continues to be ejected and to be claimed by the Kelvin-Helmholtz instability at or before $\tilde{l}$. Small scale bubbles ($\ll r_n$) will be released. The physical processes are radically different from those involved in blowing gas bubbles in liquids where viscous forces dominate over surface instabilities. Moreover, there is a basic difference between this result and numerical results that rely upon cylindrical symmetry (Wiita 1978*b*; Norman *et al.* 1981). The latter leads to the continual release of bubbles of radius $\sim r_n$ since only toroidal perturbations on the surface are allowed. We note that the overall effect of the instability on a jet is independent of wavelength, and so the minimum jet luminosity determined in § III was close to that obtained by sophisticated numerical methods (Norman *et al.* 1981).

VIII. CLOUDS

Above the critical luminosity calculated in § IV, the cavity bloats out and light gas is released in all directions through the Rayleigh-Taylor instability. This stage is reached after the inevitable collapse of the wide nozzle (Norman *et al.* 1981, Fig. 5) that leads to the ejection of a large cloud along the symmetry axis. The mass of the cloud is estimated to be $\sim 1.2\pi r_n^3 \rho_n (\rho_g/\rho_n)^{1/2}$, occupying a volume greater than the central dense gas cloud. Then smaller clouds are released through the cavity walls. If the mass lost through these lower wavelength Rayleigh-Taylor modes balances the mass ejected from the central shock, then the nozzle does not reform, i.e. saturation by these fast growing modes stops the longest wavelength mode from growing. Nozzle formation takes place when the longest wavelength mode can grow. By comparing the time scales derived from these processes in §§ II and IV, we find that the nozzle will indeed reform. The mass that can be released through small clouds is a fraction $\sim 0.3(\rho_n/\rho_g)^{1/6}$ of the total mass flow rate.

The large clouds released along the symmetry axis correspond to the clouds proposed by Gull and Northover (1973). Instead of leading to extended sources, we believe the clouds to be related to flux variations in compact radio sources. Such variations are well explained by an expanding "plasmon" model (Pacholczyk 1977 and references therein); the "plasmons" are here interpreted as clouds released from the cavity surrounding the central engine. The physical mechanism—an instability—implies that the clouds are not released periodically, but on a time scale given only by order of magnitude. This is consistent with observations. It appears that, occasionally, a source can release several plasmons almost simultaneously (Macleod, Andrew, and Medd 1971). These outbursts could correspond to the isotropic ejection of smaller clouds, intensified by the cavity bloating out further than usual. The interpretation of superluminal sources will require a relativistic version of this model to be developed. The continued high radio flux that follows the increase in emission and the ejection of a radio component (Cohen *et al.* 1977) calls for such a model. Here, an increase in power of the central engine can push a quasar into the cloud region of the L-C_0 diagram.

The lack of a class of objects permanently in the cloud region requires explanation. One possibility is that the increase in luminosity stops the fuel supply to the central engine. For instance, the small clouds can heat the central cloud gas, thus inhibiting the infall of dense filaments toward the engine.

We must also explain the lack of powerful compact radio cores within radio sources, associated with elliptical galaxies. Why are powerful radio sources associated with giant ellipticals invariably extended? We shall here attempt to answer this in terms of mass accretion from the dense central cloud. Mass accretes at the rate $\sim M_g/t_b$ through cooling in the cloud, where t_b is the bremsstrahlung cooling time scale. This gives an infall speed ξC_g, say. This accretion rate then is the maximum mass outflow rate from the central engine. This condition yields $\frac{1}{2}(r_n/l)^2(C_g/C_n) < \xi$. Consequently, when $r_n \sim 0.7l$, $\xi > \frac{1}{4}(C_g/C_n)$, requiring high radial infall speeds. If no quasisteady cavity flows can exist under such circumstances (we also note that the central cloud must rapidly replace the infalling gas), then we have an answer: in ellipticals, gas accretes directly from the dense cloud, and compact radio components of high power cannot form because of the high infall speeds required. In spiral type galaxies, we suggest that the fuel supply is from very dense and small gas clouds embedded within the central cloud. In this case we have a powerful energy supply for the compact source. Supporting evidence comes from optical spectra. Grandi and Osterbrock (1978) have shown that most broad-line radio galaxies are N galaxies, whereas most narrow-line radio galaxies are ellipticals. Thus N galaxies contain very dense clouds with virial speeds that place them close to the central cloud. In ellipticals, they appear to

© American Astronomical Society • Provided by the NASA Astrophysics Data System

1983ApJ...264..432S

be missing. The final question—why are they missing?—is beyond the tasks set in this paper. We do, however, suggest that very dense clouds can survive in the relatively fast-rotating spirals, where evaporation is suppressed by the strong magnetic fields generated through the rotation.

IX. CONCLUSION

Jet formation through the fluid twin-exhaust mechanism has been thoroughly investigated through a theoretical analysis which supports and generalizes numerical simulations (Norman *et al.* 1981). General flow features were summarized in the latter work. The results found here include:

1. Cavity-nozzle structures are expected, provided the confining central cloud is asymmetric and the pressure decreases slowly with radius ($\rho \propto r^{-m}, m < 2$). The stability of these structures is primarily dependent on the central power.

2. The nozzle breaks up through the Kelvin-Helmholtz instability when it is thin in comparison to the central cloud's pressure scale height (eq. [24]), giving a minimum jet power (eq. [25]). Below this power, a turbulent wake of bubbles streams out of the cloud along the symmetry axis.

3. The cavity-nozzle is Rayleigh-Taylor unstable, leading to nozzle choking above a maximum jet power given by equation (20). Above this power, large buoyant clouds are ejected.

4. Steady jets are formed (for a finite range of powers) only if the cavity sound speed is less than 30 times the confining cloud sound speed (Fig. 4). Eccentricity has little effect on the results (Fig. 5). Suppression of the Kelvin-Helmholtz instability (e.g., by magnetic fields) would give a less restrictive result.

5. The radio galaxy Cygnus A requires a central mass 10^9–$10^{10}\ M_\odot$, and a gas mass of $\sim 10^4\ M_\odot$ within 1 pc. Nonrelativistic sound speeds are then acceptable. The mass flow rate is $\sim 10\ M_\odot\ \mathrm{yr}^{-1}$. General application to extended sources is described elsewhere (Smith *et al.* 1981).

6. The critical dependence on the confining cloud sound speed enables us to sketch a schematic picture for active galactic nuclei. Seyfert galaxies and quasars are placed in the bubble regime as suggested by low radio powers and broad emission lines (Fig. 6).

7. We propose that the low powered bubbling gives rise to the observed radio components within a few kiloparsecs of nuclei of Seyfert galaxies. In general, sources in this regime have weak radio components.

8. Compact radio sources are interpreted by the high powered clouds, with particular reference to the expanding cloud model for flux variations in these sources.

9. Limitations on the fuel supply may explain the lack of powerful compact radio sources in elliptical galaxies. The lack of broad-line regions in most ellipticals suggests that gas must be directly accreted from the central cloud, whereas for spiral types (here including quasars), broad emission lines suggest that condensed gas clouds are available for accretion.

In this paper we have tackled the nonrelativistic problem (speeds of $0.1C$ have been used without relativistic corrections). If the central engine is producing relativistic gas, we envisage significant changes in the flow characteristics. Without sophisticated numerical simulations to guide us, we have not as yet attempted this case. Thus we have been restricted to temperatures $< 10^{10}$ K; thermal equilibrium between electrons and protons has been used throughout this paper—we note that the electron-proton equilibrium time is shorter than the cooling time for these temperatures. The possibility of pair production (Wiita 1978*a*) is a further complication. If the central cloud is optically thin, as proposed for Cygnus A, then this is unimportant. Optically thick models, including supermassive clouds, have been considered by Smith *et al.* (1981).

Angular momentum has been ignored in our stability analysis. This is in keeping with the numerical work (Norman *et al.* 1981) where the flattened self-gravitating cloud was mainly responsible for the 2:1 axial pressure ratio. In astrophysical situations, the angular momentum may be the dominant factor in cloud flattening.

Magnetic field pressure within the nozzle or cloud may be an important stabilizing influence. We have here assumed the field to be too weak to affect the dynamics. The initial expansion and shock compression will intensify the field component perpendicular to the flow. Shearing along the cavity and nozzle walls will generate a parallel field. Hence, the model is capable of producing the various field structures observed in jets (Miley 1980). Further discussions on the possible origins, resulting features, and modifications to hydrodynamic jets are given by Blandford and Rees (1978) and Rees (1980) and will not be repeated here.

We have assumed just one property of the central engine—an ability to produce hot gas. Once turned on, changes in power are presumed to be small in comparison to the flow time scale. Factors that need consideration are (1) rapid power fluctuations and (2) a central engine displaced from its position at the centroid of mass. The central engine may also be the source of high energy photons that photoionize optically thick filaments within the core.

The simplicity of the model—hot gas being ejected into a dense cloud bounded by a deep gravitational potential well—has made progress possible. The size of the central region ($\leqslant 1$ pc) leads to enormous difficulties in undertaking proposed tests. By considering possible evolutionary traits of the model developed in this paper, we hope to initiate indirect tests. We have considered the power of the central engine to increase from a low

© American Astronomical Society • Provided by the NASA Astrophysics Data System

1983ApJ...264..432S

level. In some nuclei the jet stage is reached. The nucleus spends, perhaps, 1/100 of its lifetime at this level before exhausting the fuel supply or before its efficiency at converting the fuel into hot gas is reduced. The re-ejection of mass into the galaxy can increase its lifetime through recycling. When done efficiently, i.e., through jets, its continuation is further prolonged. Consequently, we can expect jet sources to survive until the present age of the universe. Active nuclei without jets will tend to evolve much faster down to a lower level of activity. This prediction of our model is in agreement with our placement of type I and type II quasars on our schematic diagram (Fig. 6). Ku *et al.* (1980) find that type I quasars show strong evolution, while type II quasars do not.

We conclude that a variety of phenomena observed in active galactic nuclei are reproducible within the fluid twin-exhaust framework. A variety of extended jet structures has previously been found (Smith and Norman 1981). The severe constraints on jet formation are discussed in a related paper (Smith *et al.* 1981). Investigations into the origin of the dense nuclear gas and the nature of the central engine are required.

One of us (L. S.) would like to thank Martin Rees for his hospitality and stimulating discussions at the Institute of Astronomy where a portion of this work was done. F. K. Lamb provided valuable ideas and criticisms on major portions of the paper. We appreciate valuable discussions with R. D. Blandford, D. Lynden-Bell, G. Miley, C. Norman, and P. Witta. We also thank the Department of Energy and the NSF for financial support under grants PHY78-04404 and PHY80-01496, and the Center for Theoretical Physics, University of Maryland.

REFERENCES

Auriemma, C., *et al.* 1977, *Astr. Ap*, **57**, 41.
Blake, G. M. 1972, *M.N.R.A.S.*, **156**, 67.
Blandford, R. D., and McKee, C. F. 1977, *M.N.R.A.S.*., **180**, 343.
Blandford, R. D., and Pringle, J. E. 1976, *M.N.R.A.S.*, **176**, 443.
Blandford, R. D., and Rees, M. J. 1974, *M.N.R.A.S.*, **169**, 395.
_____. 1978, *Phys. Scripta*, **17**, 265.
Christiansen, W. A., and Scott, J. S. 1977, *Ap. J.* (*Letters*), **216**, L1.
Cohen, M. H., *et al.* 1977, *Nature*, **268**, 405.
Courant, R., and Friedrichs, K. O. 1948, *Supersonic Flow and Shock Waves* (New York: Interscience Publishers).
Fejer, J. A., and Miles, J. W. 1963, *J. Fluid Mech.*, **15**, 335.
Ferrari, A., Trussoni, E., and Zaninetti, L. 1978, *Astr. Ap.*, **64**, 43.
Grandi, S. A., and Osterbrock, D. E. 1978, *Ap. J.*, **220**, 783.
Gull, S. F., and Northover, K. J. E. 1973, *Nature*, **244**, 80.
Hardee, P. E. 1979, *Ap. J.*, **234**, 47.
Heckman, T. M., Miley, G. K., van Breugel, W. J. M., and Butcher, H. R. 1981, *Ap. J.*, **247**, 403.
Kafatos, M. 1978, *Ap. J.*, **225**, 756.
Ku, W. H. M., Helfand, D. J., and Lucy, L. B. 1980, *Nature*, **288**, 323.
Linfield, R., 1981, *Ap. J.*, **254**, 465.
MacLeod, J. M., Andrew, B. H., and Medd, W. J. 1971, *Ap. Letters*, **9**, 19.
Miley, G. K. 1980, *Ann. Rev. Astr. Ap.*, **18**, 165.
Miley, G. K., and Hartsuijker, 1978, *Astr. Ap. Suppl.*, **34**, 129.
Norman, M. L., Smarr, L., Wilson, J. R., and Smith, M. D. 1981, *Ap. J.*, **247**, 52.
Pacholczyk, A. G. 1977, *Radio Galaxies* (New York: Pergamon Press).
Pai, S. I. 1954, *J. Aerosol. Sci.*, **21**, 325.
Rayburn, D. R. 1977, *M.N.R.A.S.*, **179**, 603.
Readhead, A. C. S., Cohen, M. H., and Blandford, R. D. 1978, *Nature*, **272**, 131.
Rees, M. J. 1976, in *The Physics of Non-Thermal Radio Sources*, ed. G. Setti (Dordrecht: Reidel).
Sanders, R. H. 1976, *Ap. J.*, **205**, 335.
Scheuer, P. A. G. 1974, *M.N.R.A.S.*, **166**, 513.
Shapiro, P. R. 1979, *Ap. J.*, **233**, 831.
Smith, M. D., and Norman, C. A. 1981, *M.N.R.A.S.*, **194**, 771.
Smith, M. D., Smarr, L., Norman, M. L., and Wilson, J. R. 1981, *Nature*, **293**, 277.
Turland, B. D., and Scheuer, P. A. G. 1976, *M.N.R.A.S.*, **176**, 421.
Wiita, P. J. 1978*a*, *Ap. J.*, **221**, 41.
_____. 1978*b*, *Ap. J.*, **221**, 436.

MICHAEL L. NORMAN: Max-Planck-Institut für Physik und Astrophysik, Garching, München, West Germany

LARRY SMARR: Department of Astronomy, University of Illinois at Urbana-Champaign, 1110 West Springfield, Urbana, IL 61801

MICHAEL D. SMITH: Department of Astronomy, University of Leicester, University Road, Leicester LE1 7RH, England

JAMES W. WILSON: L-35, Lawrence Livermore Laboratory, P. O. Box 808, Livermore CA 94550

© American Astronomical Society • Provided by the NASA Astrophysics Data System